

ANALYSIS AND COMPUTATION OF COMPATIBLE LEAST-SQUARES METHODS FOR DIV-CURL EQUATIONS. *

PAVEL B. BOCHEV[†], KARA PETERSON[†], AND CHRISTOPHER M. SIEFERT[‡]

Abstract. We develop and analyze least-squares finite element methods for two complementary div-curl elliptic boundary value problems. The first one prescribes the tangential component of the vector field on the boundary and is solved using curl-conforming elements. The second problem specifies the normal component of the vector field and is handled by div-conforming elements.

We prove that both least-squares formulations are norm-equivalent with respect to suitable discrete norms, yield optimal asymptotic error estimates and give rise to algebraic systems that can be solved by efficient algebraic multigrid methods. Numerical results that illustrate scalability of iterative solvers and optimal rates of convergence are also included.

AMS subject classifications. 65F10, 65F30, 78A30

1. Introduction. This paper deals with development, analysis and computation of compatible least-squares finite element methods (LSFEMs) for two complementary div-curl boundary value problems. The first problem is given by

$$\begin{cases} \nabla \times \mathbf{u} = \mathbf{g} & \text{in } \Omega \\ \Theta_0^{-1} \nabla \cdot \Theta_1 \mathbf{u} = f & \text{in } \Omega \end{cases} \quad \text{and} \quad \mathbf{n} \times \mathbf{u} = 0 \quad \text{on } \Gamma. \quad (1.1)$$

LSFEM for (1.1) are developed using *curl*-conforming elements. The second div-curl problem is given by

$$\begin{cases} \Theta_1^{-1} \nabla \times \Theta_2 \mathbf{u} = \mathbf{g} & \text{in } \Omega \\ \nabla \cdot \mathbf{u} = f & \text{in } \Omega \end{cases} \quad \text{and} \quad \mathbf{n} \cdot \mathbf{u} = 0 \quad \text{on } \Gamma. \quad (1.2)$$

Accordingly, LSFEM for (1.2) employ *div*-conforming elements. See [3, 14, 31, 32] and the references therein for more details about div and curl-conforming elements.

In (1.1)–(1.2) Ω is a bounded region in \mathbb{R}^3 with Lipschitz-continuous boundary $\Gamma = \partial\Omega$, and \mathbf{g} and f are given data. In what follows, Θ_0 and Θ_3 denote given piecewise smooth scalar fields, and Θ_1 and Θ_2 are given piecewise smooth tensor fields. We assume that Θ_i are non-degenerate in the sense that there are positive real $\alpha_0, \alpha_1, \alpha_2$, and α_3 such that for $\boldsymbol{\xi} \in \mathbb{R}^3$

$$\frac{1}{\alpha_i} \leq \Theta_i \leq \alpha_i; \quad i = 0, 3 \quad \text{and} \quad \frac{1}{\alpha_i} \boldsymbol{\xi}^\top \boldsymbol{\xi} \leq \boldsymbol{\xi}^\top \Theta_i \boldsymbol{\xi} \leq \alpha_i \boldsymbol{\xi}^\top \boldsymbol{\xi}; \quad i = 1, 2. \quad (1.3)$$

The boundary value problems (1.1)–(1.2) arise either on their own or as parts in more complex mathematical models. A well-known example that has (1.1) as its prototype

*Received by the editors October 01, 2009; accepted for publication (in revised form) Month ??, 2010; published electronically Month ??, 2010. Sandia is a multiprogram laboratory operated by Sandia Corporation, a Lockheed Martin Company, for the United States Department of Energy under contract DE-AC04-94-AL85000. The U.S. Government retains a nonexclusive, royalty-free license to publish or reproduce the published form of this contribution, or allow others to do so, for U.S. Government purposes. Copyright is owned by SIAM to the extent not limited by these rights.

<http://www.siam.org/journals/sinum/?????.html>.

[†]Sandia National Laboratories, Applied Mathematics and Applications, P.O. Box 5800, MS 1320, Albuquerque, NM 87185-1320 ({pbboche, kjpeter}@sandia.gov).

[‡]Sandia National Laboratories, Computational Shock and Multiphysics, P.O. Box 5800, MS 0378, Albuquerque, NM 87185-0378 (csiefer@sandia.gov).

is the linear magnetostatics problem

$$\begin{cases} \nabla \times \mathbf{H} = \mathbf{J}_0 & \text{in } \Omega \\ \nabla \cdot \mu \mathbf{H} = 0 & \text{in } \Omega \end{cases} \quad \text{and} \quad \mathbf{n} \times \mathbf{H} = 0 \quad \text{on } \Gamma \quad (1.4)$$

in terms of the magnetic field intensity \mathbf{H} . The complementary system (1.2) is prototype of the same problem in terms of the *dual* magnetic flux density \mathbf{B} :

$$\begin{cases} \nabla \times \mu^{-1} \mathbf{B} = \mathbf{J}_0 & \text{in } \Omega \\ \nabla \cdot \mathbf{B} = 0 & \text{in } \Omega \end{cases} \quad \text{and} \quad \mathbf{n} \cdot \mathbf{B} = 0 \quad \text{on } \Gamma. \quad (1.5)$$

In (1.4)–(1.5), \mathbf{J}_0 is a given function that specifies the imposed current density and μ is the magnetic permeability.

Finite element solution of (1.1) and (1.2) is complicated by the fact that these problems are elliptic in¹ $H_0(\Omega, \text{curl}) \cap H(\Omega, \text{div})$ and $H(\Omega, \text{curl}) \cap H_0(\Omega, \text{div})$, respectively. On the one hand, it is easy to see that a finite element subspace of $H(\Omega, \text{curl}) \cap H(\Omega, \text{div})$ contains piecewise smooth fields that are both tangentially and normally continuous across the element interfaces and so, they are necessarily² in $[H^1(\Omega)]^3$; see [3, Lemma 5.1]. On the other hand, Costabel [17] has shown that unless Ω has smooth boundary or is a convex polyhedron, $H_0(\Omega, \text{curl}) \cap [H^1(\Omega)]^3$ and $H_0(\Omega, \text{div}) \cap [H^1(\Omega)]^3$ are closed, infinite-codimensional subspaces of $H_0(\Omega, \text{curl}) \cap H(\Omega, \text{div})$ and $H(\Omega, \text{curl}) \cap H_0(\Omega, \text{div})$. As a result, on such domains standard C^0 elements do not possess the approximability property; see [19, Corollary 3.20, p. 97]. Consequently, C^0 elements are a poor choice for div-curl systems.

It should be noted that the complications caused by the $H(\Omega, \text{curl}) \cap H(\Omega, \text{div})$ functional space setting are not limited to finite elements and have to be dealt with in finite difference and finite volume methods as well. Successful methods for div-curl systems resolve the issue of approximating $H(\Omega, \text{curl}) \cap H(\Omega, \text{div})$ using one of the following three strategies:

- Maintain div and curl conformity by using *topologically dual grids*. In this approach, which is typical of finite volume methods [33–35], the curl and the divergence are discretized on separate grids.
- Maintain div and curl conformity by using *two sets of variables*. Usually this approach is implemented by transforming the div-curl system into a constrained optimization problem with the L^2 error between the two variables serving as an objective functional. For instance, in magnetostatics this idea gives rise to the so-called error-based [37] or field-based [2, 15] methods in which the error in the constitutive equation $\mathbf{B} = \mu \mathbf{H}$ is minimized subject to $\nabla \times \mathbf{H} = \mathbf{J}_0$ and $\nabla \cdot \mathbf{B} = 0$.
- Maintain div *or* curl conformity using a single variable and a single grid. This approach is typical of mixed finite elements [10, 12] and mimetic finite differences [27, 28] and requires approximation of either the curl or the div operator. For example, a curl-conforming mimetic method for (1.1) uses the so-called *natural* [27] curl operator and the *adjoint* or *derived* divergence operator; see [26] for discussion of adjoint mimetic operators.

Each one of these three strategies has its advantages and disadvantages. Topological duality effectively restricts the first approach to Voronoi-Delaney or Cartesian

¹See Section 2 for notation and definitions of various function spaces.

²In other words, conforming finite element approximations of $H(\Omega, \text{curl}) \cap H(\Omega, \text{div})$ default to standard C^0 finite element spaces.

grids [33, 35]. The second approach doubles the number of the dependent variables. The derived operator in the third approach is usually not sparse and direct discretization of the div-curl system by mimetic or mixed methods yields linear algebraic systems that are not easy to solve efficiently.

The main goal of this paper is to demonstrate that some, if not all, drawbacks of the third approach can be mitigated, and all advantages retained, by switching to properly formulated *compatible* least-squares minimization principles. Resulting LSFEMs for (1.1) and (1.2) are optimally accurate and, just like mimetic or mixed methods, require a derived discrete operator. Thus, formally, least-squares algebraic systems involve a non-sparse matrix. However, we show that discrete norm-equivalence of the least-squares functional leads to symmetric and positive definite linear systems that can be solved efficiently by iterative multilevel methods developed for curl-conforming discretizations of the Maxwell's equations [7, 9]. Because such methods require only application of the matrix, lack of sparsity bears no negative impact on the practicality of LSFEMs for (1.1). This fact is confirmed by the numerical results in Section 5 which demonstrate good convergence rates and solver scalability.

The rest of the paper is organized as follows. Section 2 reviews notation, basic definitions and facts about the relevant function spaces, and their compatible finite element approximations. Section 3 introduces and analyzes the curl and div-conforming discrete least-squares principles (DLSP) for (1.1)–(1.2). Implementation of the DLSPs and multilevel solvers are considered in Section 4 and numerical results are presented in Section 5.

2. Quotation of results and notation. Throughout the paper we employ standard notation and definitions of various function spaces and operators. As usual, $L^2(\Omega)$ is the Hilbert space of all square integrable functions with inner product and norm $(\cdot, \cdot)_0$ and $\|\cdot\|_0$, respectively, and $L_0^2(\Omega)$ is the subspace of $L^2(\Omega)$ consisting of functions with zero mean. Bold face denotes vector spaces, e.g., $\mathbf{L}^2(\Omega) = [L^2(\Omega)]^3$. Formulation of dimensionally and unit consistent least-squares functionals requires two sets of function spaces that account for the weights in (1.1) and (1.2). These spaces are defined using the weighted L^2 norms

$$\|u\|_{0,\Theta}^2 = (\Theta u, u)_0 = (u, u)_{0,\Theta}, \quad (2.1)$$

and the associated weighted L^2 spaces $L^2(\Omega, \Theta)$, where Θ is a piecewise smooth, non-degenerate weight function. The first set consists of the spaces

$$H_0^1(\Omega, \Theta_0) = \{u \in L^2(\Omega, \Theta_0) \mid \nabla u \in L^2(\Omega, \Theta_1); u = 0 \text{ on } \Gamma\}, \quad (2.2)$$

$$H_0(\Omega, \text{curl}, \Theta_1) = \{\mathbf{u} \in \mathbf{L}^2(\Omega, \Theta_1) \mid \nabla \times \mathbf{u} \in L^2(\Omega, \Theta_2); \mathbf{u} \times \mathbf{n} = 0 \text{ on } \Gamma\}, \quad (2.3)$$

$$H_0(\Omega, \text{div}, \Theta_2) = \{\mathbf{u} \in \mathbf{L}^2(\Omega, \Theta_2) \mid \nabla \cdot \mathbf{u} \in L_0^2(\Omega, \Theta_3); \mathbf{u} \cdot \mathbf{n} = 0 \text{ on } \Gamma\}, \quad (2.4)$$

equipped with the graph norms

$$\begin{aligned} \|u\|_G^2 &= \|u\|_{0,\Theta_0}^2 + \|\nabla u\|_{0,\Theta_1}^2 & \|\mathbf{u}\|_C^2 &= \|u\|_{0,\Theta_1}^2 + \|\nabla \times \mathbf{u}\|_{0,\Theta_2}^2, \\ \text{and } \|\mathbf{u}\|_D^2 &= \|\mathbf{u}\|_{0,\Theta_2}^2 + \|\nabla \cdot \mathbf{u}\|_{0,\Theta_3}^2, \end{aligned} \quad (2.5)$$

respectively, and the space $L_0^2(\Omega, \Theta_3)$. The second set is defined by making the substitutions $\Theta_0 \rightarrow \Theta_3^{-1}$; $\Theta_1 \rightarrow \Theta_2^{-1}$, $\Theta_2 \rightarrow \Theta_1^{-1}$, and $\Theta_3 \rightarrow \Theta_0^{-1}$ in (2.2)–(2.5).

To denote the versions of (2.2)–(2.4) without the boundary conditions imposed we drop the subscript 0 from the space designation.

REMARK 1. For unit weights the so defined function spaces coincide with the standard definitions of $H_0^1(\Omega)$, $H_0(\Omega, \text{curl})$, $H_0(\Omega, \text{div})$ and $L_0^2(\Omega)$, respectively. Moreover, because all weights are assumed non-degenerate, norms in (2.1) and (2.5) are equivalent to the standard norms, and basic inequalities valid for the standard spaces extend to (2.2)–(2.4), possibly with a different constant.

The space $H_t(\Theta_1) = H_0(\Omega, \text{curl}, \Theta_1) \cap H(\Omega, \text{div}, \Theta_1^{-1})$, endowed with norm

$$\|\mathbf{u}\|_{H_t(\Theta_1)}^2 = \|\mathbf{u}\|_{0,\Theta_1}^2 + \|\nabla \times \mathbf{u}\|_{0,\Theta_2}^2 + \|\nabla \cdot \Theta_1 \mathbf{u}\|_{0,\Theta_0^{-1}}^2. \quad (2.6)$$

provides the functional setting for (1.1). Likewise, $H_n(\Theta_2) = H(\Omega, \text{curl}, \Theta_2^{-1}) \cap H(\Omega, \text{div}, \Theta_2)$ with norm

$$\|\mathbf{u}\|_{H_n(\Theta_2)}^2 = \|\mathbf{u}\|_{0,\Theta_2}^2 + \|\nabla \times \Theta_2 \mathbf{u}\|_{0,\Theta_1^{-1}}^2 + \|\nabla \cdot \mathbf{u}\|_{0,\Theta_3}^2. \quad (2.7)$$

provides the setting for (1.2). We recall the Poincaré–Friedrichs inequality

$$\|\mathbf{u}\|_0 \leq C_P (\|\nabla \times \mathbf{u}\|_0 + \|\nabla \cdot \mathbf{u}\|_0), \quad (2.8)$$

that holds for all $\mathbf{u} \in H_0(\Omega, \text{curl}) \cap H(\Omega, \text{div})$ and $\mathbf{u} \in H(\Omega, \text{curl}) \cap H_0(\Omega, \text{div})$. From (2.8) and Remark 1 it follows that

$$\|\mathbf{u}\|_{H_t(\Theta_1)} \leq C \left(\|\nabla \times \mathbf{u}\|_{0,\Theta_2} + \|\nabla \cdot \Theta_1 \mathbf{u}\|_{0,\Theta_0^{-1}} \right), \quad (2.9)$$

for all $\mathbf{u} \in H_t(\Theta_1)$, and

$$\|\mathbf{u}\|_{H_n(\Theta_2)} \leq C \left(\|\nabla \times \Theta_2 \mathbf{u}\|_{0,\Theta_1^{-1}} + \|\nabla \cdot \mathbf{u}\|_{0,\Theta_3} \right), \quad (2.10)$$

for all $\mathbf{u} \in H_n(\Theta_2)$. Consequently, the right hand sides in (2.9) and (2.10) define equivalent norms on $H_t(\Theta_1)$ and $H_n(\Theta_2)$, denoted by $\|\cdot\|_t$ and $\|\cdot\|_n$, respectively.

Throughout the paper we assume that Ω is a bounded contractible region and so, the DeRham complex

$$\mathbb{R} \hookrightarrow H_0^1(\Omega) \xrightarrow{\nabla} H_0(\Omega, \text{curl}) \xrightarrow{\nabla \times} H_0(\Omega, \text{div}) \xrightarrow{\nabla \cdot} L_0^2(\Omega) \longrightarrow 0, \quad (2.11)$$

and its weighted space analogues are exact; see [3].

We formulate compatible LSFEMs for the div-curl system (1.1) using spaces from a finite element DeRham complex that approximates (2.11). Such a complex is comprised of conforming finite element subspaces $G_0^h(\Omega) \subset H_0^1(\Omega)$, $\mathbf{C}_0^h(\Omega) \subset H_0(\Omega, \text{curl})$, $\mathbf{D}_0^h(\Omega) \subset H_0(\Omega, \text{div})$ and $S_0^h(\Omega) \subset L_0^2(\Omega)$ that form an exact sequence, and bounded projection operators $\Pi_G : H_0^1(\Omega) \mapsto G_0^h(\Omega)$, $\Pi_C : H_0(\Omega, \text{curl}) \mapsto \mathbf{C}_0^h(\Omega)$, $\Pi_D : H_0(\Omega, \text{div}) \mapsto \mathbf{D}_0^h(\Omega)$, and $\Pi_S : L_0^2(\Omega) \mapsto S_0^h(\Omega)$ such that the diagrams

$$\begin{array}{ccccccc} H_0^1(\Omega) & \xrightarrow{\nabla} & H_0(\Omega, \text{curl}) & \xrightarrow{\nabla \times} & H_0(\Omega, \text{div}) & \xrightarrow{\nabla \cdot} & L_0^2(\Omega) \\ \Pi_G \downarrow & & \Pi_C \downarrow & & \Pi_D \downarrow & & \Pi_S \downarrow \\ G_0^h(\Omega) & \xrightarrow{\nabla} & \mathbf{C}_0^h(\Omega) & \xrightarrow{\nabla \times} & \mathbf{D}_0^h(\Omega) & \xrightarrow{\nabla \cdot} & S_0^h(\Omega) \end{array} \quad (2.12)$$

commute. The standard $L^2(\Omega)$ projections onto compatible finite element spaces are denoted by π_G , π_C , π_D and π_S .

For simplicity, we restrict attention to partitions \mathcal{T}_h of Ω into affine simplicial elements κ because construction of the requisite finite element spaces in this case

is fairly straightforward [3, 16]. This assumption obviates the need to account for technical details that are unimportant for the development of the LSFEMs.

In this case, $G_0^h(\Omega)$ is the familiar C^0 piecewise polynomial space and $S_0^h(\Omega)$ is a discontinuous piecewise polynomial space. Henceforth these are denoted by $G_0^r(\Omega)$ and $S_0^r(\Omega)$, respectively, where $r \geq 1$ is the polynomial degree. There are more choices for $\mathbf{C}_0^h(\Omega)$ and $\mathbf{D}_0^h(\Omega)$ but here we restrict attention to curl and div conforming elements of the first and the second kinds; see [31, 32]. The former are denoted by $\mathbf{C}_0^{r-}(\Omega)$ and $\mathbf{D}_0^r(\Omega)$, respectively, whereas $\mathbf{C}_0^r(\Omega)$ and $\mathbf{D}_0^r(\Omega)$ stand for elements of the second kind. In both cases $r \geq 1$ is an integer related to the polynomial degree used to define the spaces.

Although approximation properties of these spaces are well-known [3, 13, 14, 31, 32] we review them for completeness. Below Π_X^r and π_X^r stand for bounded and L^2 projection operators onto the respective finite element spaces, indexed by an integer $r \geq 1$. First we have that for every $u \in H^{r+1}(\Omega)$,

$$\left. \begin{array}{l} \|u - \Pi_G^r u\|_0 \\ \|u - \pi_G^r u\|_0 \\ \|u - \pi_S^r u\|_0 \end{array} \right\} \leq Ch^{r+1} \|u\|_{r+1} \quad \text{and} \quad \|\nabla(u - \Pi_G^r u)\|_0 \leq Ch^r \|\nabla u\|_r. \quad (2.13)$$

Furthermore, given a vector field $\mathbf{u} \in \mathbf{H}^{r+1}(\Omega)$,

$$\left. \begin{array}{l} \|\mathbf{u} - \Pi_C^r \mathbf{u}\|_0 \\ \|\mathbf{u} - \pi_C^r \mathbf{u}\|_0 \end{array} \right\} \leq C \begin{cases} h^r \|\mathbf{u}\|_r & \text{if } \mathbf{C}^h(\Omega) = \mathbf{C}^{r-}(\Omega) \\ h^{r+1} \|\mathbf{u}\|_{r+1} & \text{if } \mathbf{C}^h(\Omega) = \mathbf{C}^r(\Omega) \end{cases} \quad (2.14)$$

$$\|\nabla \times (\mathbf{u} - \Pi_C^r \mathbf{u})\|_0 \leq Ch^r \|\nabla \times \mathbf{u}\|_r,$$

and

$$\left. \begin{array}{l} \|\mathbf{u} - \Pi_D^r \mathbf{u}\|_0 \\ \|\mathbf{u} - \pi_D^r \mathbf{u}\|_0 \end{array} \right\} \leq C \begin{cases} h^r \|\mathbf{u}\|_r & \text{if } \mathbf{D}^h(\Omega) = \mathbf{D}^{r-}(\Omega) \\ h^{r+1} \|\mathbf{u}\|_{r+1} & \text{if } \mathbf{D}^h(\Omega) = \mathbf{D}^r(\Omega) \end{cases} \quad (2.15)$$

$$\|\nabla \cdot (\mathbf{u} - \Pi_D^r \mathbf{u})\|_0 \leq Ch^r \|\nabla \cdot \mathbf{u}\|_r.$$

Compatible LSFEMs require discrete approximations of curl and div acting on $\mathbf{D}_0^h(\Omega)$ and $\mathbf{C}_0^h(\Omega)$, respectively. The operator $\nabla_h^* \times : \mathbf{D}_0^h(\Omega) \mapsto \mathbf{C}_0^h(\Omega)$ is defined by

$$(\nabla_h^* \times \mathbf{v}^h, \mathbf{u}^h)_{0, \Theta_1} = (\mathbf{v}^h, \nabla \times \mathbf{u}^h)_{0, \Theta_2} - \int_{\Gamma} (\mathbf{n} \times \Theta_2 \mathbf{v}^h) \cdot \mathbf{u}^h d\Gamma \quad \forall \mathbf{u}^h \in \mathbf{C}_0^h(\Omega). \quad (2.16)$$

The discrete divergence $\nabla_h^* \cdot : \mathbf{C}_0^h(\Omega) \mapsto G_0^h(\Omega)$ is given by

$$(\nabla_h^* \cdot \mathbf{u}^h, q^h)_{0, \Theta_0} = (\mathbf{u}^h, -\nabla q^h)_{0, \Theta_1} + \int_{\Gamma} (\mathbf{n} \cdot \Theta_1 \mathbf{u}^h) q d\Gamma \quad \forall q^h \in G_0^h(\Omega). \quad (2.17)$$

In what follows we assume that finite element spaces entering definitions (2.16) and (2.17) belong to the same finite element DeRham complex. This assumption has two important consequences. First; see [6, Theorem B.25, p.580], one can show that there is a constant \tilde{C}_P , independent of h , such that

$$\|\mathbf{u}^h\|_{0, \Theta_1} \leq \tilde{C}_P (\|\nabla \times \mathbf{u}^h\|_{0, \Theta_2} + \|\nabla_h^* \cdot \mathbf{u}^h\|_{0, \Theta_0}) \quad \forall \mathbf{u}^h \in \mathbf{C}_0^h(\Omega) \quad (2.18)$$

and

$$\|\mathbf{u}^h\|_{0, \Theta_2} \leq \tilde{C}_P (\|\nabla_h^* \times \mathbf{u}^h\|_{0, \Theta_1} + \|\nabla \cdot \mathbf{u}^h\|_{0, \Theta_3}) \quad \forall \mathbf{u}^h \in \mathbf{D}_0^h(\Omega), \quad (2.19)$$

i.e., discrete versions of Poincaré–Friedrichs inequalities (2.9)–(2.10) hold on $\mathbf{C}_0^h(\Omega)$ and $\mathbf{D}_0^h(\Omega)$. Second, functions in $\mathbf{C}_0^h(\Omega)$ and $\mathbf{D}_0^h(\Omega)$ admit discrete Hodge decompositions that can be expressed in terms of (2.16) and (2.17) in a way that mimics the true Hodge decomposition of vector fields. For the sake of completeness we include the full statement of the relevant results.

THEOREM 2.1 ([6, Theorem B.22, p.577]). *Let $N_0^h(\nabla \times)$ and $N_0^h(\nabla \times)^\perp$ denote the null-space of curl in $\mathbf{C}_0^h(\Omega)$ and its orthogonal complement in that space, respectively. Every $\mathbf{u}^h \in \mathbf{C}_0^h(\Omega)$ can be written as*

$$\mathbf{u}^h = \mathbf{u}_N^h + \mathbf{u}_{N^\perp}^h \quad \text{with} \quad \mathbf{u}_N^h \in N_0^h(\nabla \times) \quad \text{and} \quad \mathbf{u}_{N^\perp}^h \in N_0^h(\nabla \times)^\perp, \quad (2.20)$$

where $\nabla_h^* \cdot \mathbf{u}_{N^\perp}^h = 0$, $\mathbf{u}_{N^\perp}^h = \nabla_h^* \times \mathbf{w}^h$ for some $\mathbf{w}^h \in \mathbf{D}_0^h(\Omega)$, and $\mathbf{u}_N^h = \nabla p^h$ for some $p^h \in G_0^h(\Omega)$. Furthermore, there is a positive constant C , independent of h , such that

$$\begin{aligned} \|\mathbf{u}_{N^\perp}^h\|_0 &\leq C \|\nabla \times \mathbf{u}^h\|_0, \\ \|\mathbf{u}_N^h\|_0 &\leq C \|\nabla_h^* \cdot \mathbf{u}^h\|_0, \quad \text{and} \quad \|\mathbf{u}_N^h\|_0 \leq C \|\mathbf{u}^h\|_0. \end{aligned} \quad (2.21)$$

The result for div-conforming spaces is similar.

THEOREM 2.2 ([6, Theorem B.23, p.578]). *Let $N_0^h(\nabla \cdot)$ and $N_0^h(\nabla \cdot)^\perp$ denote the null-space of div in $\mathbf{D}_0^h(\Omega)$ and its orthogonal complement in that space, respectively. Every $\mathbf{u}^h \in \mathbf{D}_0^h(\Omega)$ can be written as*

$$\mathbf{u}^h = \mathbf{u}_N^h + \mathbf{u}_{N^\perp}^h \quad \text{with} \quad \mathbf{u}_N^h \in N_0^h(\nabla \cdot) \quad \text{and} \quad \mathbf{u}_{N^\perp}^h \in N_0^h(\nabla \cdot)^\perp, \quad (2.22)$$

where $\nabla_h^* \times \mathbf{u}_{N^\perp}^h = 0$, $\mathbf{u}_{N^\perp}^h = \nabla_h^* p^h$ for some $p^h \in S_0^h(\Omega)$, and $\mathbf{u}_N^h = \nabla \times \mathbf{w}^h$, and $\mathbf{w}^h \in \mathbf{C}_0^h(\Omega)$ is such that $\nabla_h^* \cdot \mathbf{w} = 0$. Furthermore, there exists a positive constant C , independent of h , such that

$$\begin{aligned} \|\mathbf{u}_{N^\perp}^h\|_0 &\leq C \|\nabla \cdot \mathbf{u}^h\|_0, \\ \|\mathbf{u}_N^h\|_0 &\leq C \|\nabla_h^* \times \mathbf{u}^h\|_0, \quad \text{and} \quad \|\mathbf{u}_N^h\|_0 \leq C \|\mathbf{u}^h\|_0. \end{aligned} \quad (2.23)$$

Finally, we note that the action of $\nabla_h^* \times$, and $\nabla_h^* \cdot$ can be extended to $H(\Omega, \text{div})$ and $H(\Omega, \text{curl})$. In this case it is easy to see that for sufficiently smooth \mathbf{u}

$$\nabla_h^* \times \mathbf{u} = \pi_C(\nabla \times \mathbf{u}) \quad \text{and} \quad \nabla_h^* \cdot \mathbf{u} = \pi_G(\nabla \cdot \mathbf{u}). \quad (2.24)$$

3. Discrete least-squares principles for div-curl systems. Using (2.9) it is straightforward to show; see [6, Section 3.2], that the least-squares principle

$$\begin{cases} \min_{\mathbf{u} \in H_t(\Theta_1)} J_t(\mathbf{u}; \mathbf{g}, f) \\ J_t(\mathbf{u}; \mathbf{g}, f) = \|\nabla \times \mathbf{u} - \mathbf{g}\|_{0, \Theta_2}^2 + \|\nabla \cdot \Theta_1 \mathbf{u} - f\|_{0, \Theta_1^{-1}}^2 \end{cases} \quad (3.1)$$

has a unique minimizer which solves (1.1). Likewise, from (2.10) easily follows that

$$\begin{cases} \min_{\mathbf{u} \in H_n(\Theta_2)} J_n(\mathbf{u}; \mathbf{g}, f) \\ J_n(\mathbf{u}; \mathbf{g}, f) = \|\nabla \times \Theta_2 \mathbf{u} - \mathbf{g}\|_{0, \Theta_1^{-1}}^2 + \|\nabla \cdot \mathbf{u} - f\|_{0, \Theta_3}^2 \end{cases} \quad (3.2)$$

has a unique minimizer that solves (1.2). Formally, by restricting minimization in (3.1) and (3.2) to conforming subspaces $H_t^h \subset H_t(\Theta_1)$ and $H_n^h \subset H_n(\Theta_2)$ one obtains a well-posed LSFEM; see [6, Theorem 3.28, p.92].

Unfortunately, as we have already explained in Section 1, conforming finite element subspaces of $H_0(\Omega, \text{curl}) \cap H(\Omega, \text{div})$, $H(\Omega, \text{curl}) \cap H_0(\Omega, \text{div})$ and, of course, of $H_t(\Theta_1)$ and $H_n(\Theta_2)$, default to C^0 finite elements. Consequently, notwithstanding their well-posedness, conforming discretizations of (3.1)–(3.2) are not very useful. To resolve this problem, we propose to abandon “fully” conforming approximations of $H_t(\Theta_1)$ and $H_n(\Theta_2)$ in favor of “partially” conforming finite element subspaces that are natural for the boundary conditions in the div-curl systems.

Specifically, we approximate $H_t(\Theta_1)$ by the curl-conforming space $\mathbf{C}_0^h(\Omega)$ and $H_n(\Theta_2)$ - by the div-conforming space $\mathbf{D}_0^h(\Omega)$. Of course, this means that in (3.1) divergence has to be replaced by the discrete operator defined in (2.17), so that the “partially” conforming discretization of (3.1) is given by

$$\left\{ \begin{array}{l} \min_{\mathbf{u}^h \in \mathbf{C}_0^h(\Omega)} J_t^h(\mathbf{u}^h; \mathbf{g}, f) \\ J_t^h(\mathbf{u}^h; \mathbf{g}, f) = \|\nabla \times \mathbf{u}^h - \mathbf{g}\|_{0, \Theta_2}^2 + \|\nabla_h^* \cdot \mathbf{u}^h - f\|_{0, \Theta_0}^2. \end{array} \right. \quad (3.3)$$

A “partially” conforming discretization of (3.2) uses the operator in (2.16):

$$\left\{ \begin{array}{l} \min_{\mathbf{u}^h \in \mathbf{D}_0^h(\Omega)} J_n^h(\mathbf{u}^h; \mathbf{g}, f) \\ J_n^h(\mathbf{u}^h; \mathbf{g}, f) = \|\nabla_h^* \times \mathbf{u}^h - \mathbf{g}\|_{0, \Theta_1}^2 + \|\nabla \cdot \mathbf{u}^h - f\|_{0, \Theta_3}^2. \end{array} \right. \quad (3.4)$$

REMARK 2. *Because (3.3) and (3.4) use discrete operators, their formulation requires two finite element spaces: a minimization space where the least-squares minimizer is sought, and an auxiliary space to define the discrete operator. For (3.3) this pair is given by $\{\mathbf{C}_0^h(\Omega), G_0^h(\Omega)\}$ and for (3.4) - by $\{\mathbf{D}_0^h(\Omega), \mathbf{C}_0^h(\Omega)\}$.*

3.1. Stability of discrete least-squares formulations. Because (3.3) and (3.4) use non-conforming approximations of $H_t(\Theta_1)$ and $H_n(\Theta_2)$ their stability cannot be inferred from (2.9) and (2.10). Instead, we use properties of compatible finite element spaces to establish this fact directly. To this end, define the discrete norms

$$\|\mathbf{u}^h\|_{H_t^h}^2 = \|\mathbf{u}^h\|_{0, \Theta_1}^2 + \|\nabla \times \mathbf{u}^h\|_{0, \Theta_2}^2 + \|\nabla_h^* \cdot \mathbf{u}^h\|_{0, \Theta_0}^2 \quad \forall \mathbf{u}^h \in \mathbf{C}_0^h(\Omega), \quad (3.5)$$

and

$$\|\mathbf{u}^h\|_{H_n^h}^2 = \|\mathbf{u}^h\|_{0, \Theta_2}^2 + \|\nabla_h^* \times \mathbf{u}^h\|_{0, \Theta_1}^2 + \|\nabla \cdot \mathbf{u}^h\|_{0, \Theta_3}^2 \quad \forall \mathbf{u}^h \in \mathbf{D}_0^h(\Omega). \quad (3.6)$$

We have the following equivalence result.

THEOREM 3.1. *There exists a positive constant C , independent of h , such that*

$$C\|\mathbf{u}^h\|_{H_t^h} \leq \|\nabla \times \mathbf{u}^h\|_{0, \Theta_2}^2 + \|\nabla_h^* \cdot \mathbf{u}^h\|_{0, \Theta_0}^2 \quad \forall \mathbf{u}^h \in \mathbf{C}_0^h(\Omega) \quad (3.7)$$

and

$$C\|\mathbf{u}^h\|_{H_n^h}^2 \leq \|\nabla_h^* \times \mathbf{u}^h\|_{0, \Theta_1}^2 + \|\nabla \cdot \mathbf{u}^h\|_{0, \Theta_3}^2 \quad \forall \mathbf{u}^h \in \mathbf{D}_0^h(\Omega). \quad (3.8)$$

Proof. Follows directly from the discrete Poincaré inequalities (2.18)–(2.19). \square

Theorem 3.1 implies that $J_t^h(\mathbf{u}^h; 0, 0)$ and $J_n^h(\mathbf{u}^h; 0, 0)$ define norms that are equivalent to $\|\cdot\|_{H_t^h}$ and $\|\cdot\|_{H_n^h}$, respectively. This fact is sufficient to guarantee that (3.3) and (3.4) have unique minimizers; see [6, Theorem 3.17, p.82].

3.2. Error analysis. This section establishes asymptotic error estimates for the solutions of (3.3) and (3.4). We restrict attention to the case when $f = 0$ in (1.1) and (1.2) because this is of most interest in practical applications. The assumptions that \mathcal{T}_h is a regular partition of Ω into affine simplicial elements and that (2.17)–(2.16) are defined using spaces from the same finite element DeRham complex remain in full force. We begin with the curl-conforming LSFEM (3.3).

THEOREM 3.2. *Assume that $\Omega \subset \mathbb{R}^3$ is a bounded, contractible domain with Lipschitz continuous boundary and $\mathbf{u} \in H_t(\Theta_1)$ is a solution of (1.1) with $f = 0$. Let $\mathbf{u}^h \in \mathbf{C}_0^h(\Omega)$ denote the minimizer of the LSFEM (3.3). Then,*

$$\begin{cases} \|\nabla \times (\mathbf{u} - \mathbf{u}^h)\|_0 \leq \inf_{\mathbf{v}^h \in \mathbf{C}_0^h(\Omega)} \|\nabla \times (\mathbf{u} - \mathbf{v}^h)\|_0 \\ \|\nabla \cdot \mathbf{u} - \nabla_h^* \cdot \mathbf{u}^h\|_0 \leq \|\nabla \cdot \mathbf{u} - \pi_G(\nabla \cdot \mathbf{u})\|_0, \end{cases} \quad (3.9)$$

where π_G is the L^2 projection onto the space $G_0^h(\Omega)$ entering definition (2.17).

Proof. For clarity we set all weights to one. The Euler-Lagrange equation for (3.3) is given by the weak problem: seek $\mathbf{u}^h \in \mathbf{C}_0^h(\Omega)$ such that

$$(\nabla \times \mathbf{u}^h, \nabla \times \mathbf{v}^h) + (\nabla_h^* \cdot \mathbf{u}^h, \nabla_h^* \cdot \mathbf{v}^h) = (\mathbf{g}, \nabla \times \mathbf{v}^h) \quad \forall \mathbf{v}^h \in \mathbf{C}_0^h(\Omega). \quad (3.10)$$

From Theorem 2.1, $\mathbf{v}^h = \mathbf{v}_N + \mathbf{v}_{N^\perp}$, where $\nabla \times \mathbf{v}_N = 0$ and $\nabla_h^* \cdot \mathbf{v}_{N^\perp} = 0$. Because $\nabla \times \mathbf{v}^h = \nabla \times \mathbf{v}_{N^\perp}$ and $\nabla_h^* \cdot \mathbf{v}^h = \nabla_h^* \cdot \mathbf{v}_N$ it is easy to see that (3.10) splits into two independent equations:

$$\begin{cases} (\nabla \times \mathbf{u}^h, \nabla \times \mathbf{v}^h) = (\mathbf{g}, \nabla \times \mathbf{v}^h) \\ (\nabla_h^* \cdot \mathbf{u}^h, \nabla_h^* \cdot \mathbf{v}^h) = 0 \end{cases} \quad \forall \mathbf{v}^h \in \mathbf{C}_0^h(\Omega). \quad (3.11)$$

Solution of (1.1) satisfies $\nabla \times \mathbf{u} = \mathbf{g}$ and $\nabla \cdot \mathbf{u} = 0$ and so,

$$\begin{cases} (\nabla \times \mathbf{u}^h - \nabla \times \mathbf{u}, \nabla \times \mathbf{v}^h) = 0 \\ (\nabla_h^* \cdot \mathbf{u}^h - \nabla \cdot \mathbf{u}, \nabla_h^* \cdot \mathbf{v}^h) = 0 \end{cases} \quad \forall \mathbf{v}^h \in \mathbf{C}_0^h(\Omega). \quad (3.12)$$

From the first equation in (3.12) it follows, in the usual manner, that

$$\|\nabla \times \mathbf{u}^h - \nabla \times \mathbf{u}\|_0 \leq \|\nabla \times \mathbf{v}^h - \nabla \times \mathbf{u}\|_0$$

for all $\mathbf{v}^h \in \mathbf{C}_0^h(\Omega)$. Therefore,

$$\|\nabla \times \mathbf{u}^h - \nabla \times \mathbf{u}\|_0 \leq \inf_{\mathbf{v}^h \in \mathbf{C}_0^h(\Omega)} \|\nabla \times \mathbf{v}^h - \nabla \times \mathbf{u}\|_0.$$

From the second equation in (3.12) we obtain the inequality

$$\|\nabla_h^* \cdot \mathbf{u}^h - \nabla \cdot \mathbf{u}\|_0 \leq \|\nabla_h^* \cdot \mathbf{u} - \nabla \cdot \mathbf{u}\|_0,$$

which, in conjunction with the second identity in (2.24), yields the error bound

$$\|\nabla_h^* \cdot \mathbf{u}^h - \nabla \cdot \mathbf{u}\|_0 \leq \|\pi_G(\nabla \cdot \mathbf{u}) - \nabla \cdot \mathbf{u}\|_0.$$

This completes the proof of the theorem. \square

COROLLARY 3.3. *Let $r \geq 1$ be an integer. Assume that LSFEM (3.3) is defined using either $\{\mathbf{C}_0^r(\Omega), G_0^{r+1}(\Omega)\}$ or $\{\mathbf{C}_0^{r-}(\Omega), G_0^r(\Omega)\}$ (see Remark 2), and that $\mathbf{u} \in H_0(\Omega, \text{curl}) \cap \mathbf{H}^{r+1}(\Omega)$. Then,*

$$\|\nabla \times (\mathbf{u} - \mathbf{u}^h)\|_0 + \|\nabla \cdot \mathbf{u} - \nabla_h^* \cdot \mathbf{u}^h\|_0 \leq Ch^r (\|\nabla \times \mathbf{u}\|_r + \|\nabla \cdot \mathbf{u}\|_r). \quad (3.13)$$

If (3.3) is defined using the first pair and $\mathbf{u} \in H_0(\Omega, \text{curl}) \cap \mathbf{H}^{r+3}(\Omega)$ or (3.3) is defined using the second pair and $\mathbf{u} \in H_0(\Omega, \text{curl}) \cap \mathbf{H}^{r+2}(\Omega)$, divergence error can be improved to

$$\|\nabla \cdot \mathbf{u} - \nabla_h^* \cdot \mathbf{u}^h\|_0 \leq C \begin{cases} h^{r+2} \|\nabla \cdot \mathbf{u}\|_{r+2} & \text{if } G_0^h(\Omega) = G_0^{r+1}(\Omega) \\ h^{r+1} \|\nabla \cdot \mathbf{u}\|_{r+1} & \text{if } G_0^h(\Omega) = G_0^r(\Omega). \end{cases} \quad (3.14)$$

Proof. Theorem 3.2 requires that the pairs used to define (3.3) come from the same finite element DeRham complex. Both $\{\mathbf{C}_0^r(\Omega), G_0^{r+1}(\Omega)\}$ and $\{\mathbf{C}_0^{r-}(\Omega), G_0^r(\Omega)\}$ satisfy this condition; see [3], and so, error bound (3.9) holds for \mathbf{u}^h and \mathbf{u} . If $\mathbf{u} \in H_0(\Omega, \text{curl}) \cap \mathbf{H}^{r+1}(\Omega)$, then from (2.14) it follows that

$$\inf_{\mathbf{v}^h \in \mathbf{C}_0^h(\Omega)} \|\nabla \times (\mathbf{u} - \mathbf{v}^h)\|_0 \leq Ch^r \|\nabla \times \mathbf{u}\|_r,$$

for both choices of the minimization space $\mathbf{C}_0^h(\Omega)$, whereas (2.13) implies that

$$\|\nabla \cdot \mathbf{u} - \pi_G(\nabla \cdot \mathbf{u})\|_0 \leq Ch^r \|\nabla \cdot \mathbf{u}\|_r,$$

for both choices of the auxiliary space $G_0^h(\Omega)$. This proves (3.13). When \mathbf{u} has the additional regularity stipulated in the statement of the corollary, the order of the curl approximation does not improve because it is already the best possible order for $\mathbf{C}_0^r(\Omega)$ and $\mathbf{C}_0^{r-}(\Omega)$. However, the order of the divergence approximation does increase according to (2.13). \square

The analysis of (3.4) follows along the same lines.

THEOREM 3.4. *Assume that $\Omega \subset \mathbb{R}^3$ is a bounded, contractible domain with Lipschitz continuous boundary and $\mathbf{u} \in H_n(\Theta_2)$ is a solution of (1.2) with $f = 0$. Let $\mathbf{u}^h \in \mathbf{D}_0^h(\Omega)$ denote the minimizer of the LSFEM (3.4). Then,*

$$\begin{aligned} \|\nabla \cdot (\mathbf{u} - \mathbf{u}^h)\|_0 &\leq \inf_{\mathbf{v}^h \in \mathbf{D}_0^h(\Omega)} \|\nabla \cdot (\mathbf{u} - \mathbf{v}^h)\|_0 \\ \|\nabla \times \mathbf{u} - \nabla_h^* \times \mathbf{u}^h\|_0 &\leq \|\nabla \times \mathbf{u} - \pi_C(\nabla \times \mathbf{u})\|_0, \end{aligned} \quad (3.15)$$

where π_C is the L^2 projection onto the space $\mathbf{C}_0^h(\Omega)$ entering definition (2.16).

Proof. The proof is very similar to the proof of Theorem 3.2 but uses the Hodge decomposition for $\mathbf{D}_0^h(\Omega)$ given in Theorem 2.2. \square

Similar to Theorem 3.2, the proof of Theorem 3.4 also relies on the assumption that the spaces in $\{\mathbf{D}_0^h(\Omega), \mathbf{C}_0^h(\Omega)\}$ are from the same finite element DeRham complex. However, the number of pairs $\{\mathbf{D}_0^h(\Omega), \mathbf{C}_0^h(\Omega)\}$ that fulfill this condition is greater than the number of pairs for (3.3), because there are two distinct families of div and curl-conforming elements. We refer to [3] for demonstration that the pairs

$$\mathbf{D}_0^{r-}(\Omega) \times \begin{cases} \mathbf{C}_0^r(\Omega) & \text{(I)} \\ \mathbf{C}_0^r(\Omega) & \text{(II)} \end{cases} \quad \mathbf{D}_0^r(\Omega) \times \begin{cases} \mathbf{C}_0^{(r+1)-}(\Omega) & \text{(III)} \\ \mathbf{C}_0^{r+1}(\Omega) & \text{(IV)}. \end{cases} \quad (3.16)$$

satisfy the above assumption. For sufficiently smooth solutions of (1.2), we have an analogue of Corollary 3.3.

COROLLARY 3.5. *Let $r \geq 1$ be an integer. Assume that LSFEM (3.3) is defined using one of the pairs in (3.16) and that $\mathbf{u} \in H_0(\Omega, \text{div}) \cap \mathbf{H}^{r+1}(\Omega)$. Then,*

$$\|\nabla \cdot (\mathbf{u} - \mathbf{u}^h)\|_0 + \|\nabla \times \mathbf{u} - \nabla_h^* \times \mathbf{u}^h\|_0 \leq Ch^r (\|\nabla \cdot \mathbf{u}\|_r + \|\nabla \times \mathbf{u}\|_r). \quad (3.17)$$

If (3.4) is defined using (II) or (III) and $\mathbf{u} \in H_0(\Omega, \text{div}) \cap \mathbf{H}^{r+2}(\Omega)$ or (3.4) is defined using (IV) and $\mathbf{u} \in H_0(\Omega, \text{div}) \cap \mathbf{H}^{r+3}(\Omega)$, the error estimate for the curl can be improved to

$$\|\nabla \times \mathbf{u} - \nabla_h^* \times \mathbf{u}^h\|_0 \leq C \begin{cases} h^{r+1} \|\nabla \times \mathbf{u}\|_{r+1} & \text{for (II) and (III)} \\ h^{r+2} \|\nabla \times \mathbf{u}\|_{r+2} & \text{for (IV)}. \end{cases} \quad (3.18)$$

Proof. Using the error bound (3.15) in conjunction with (2.15) gives

$$\inf_{\mathbf{v}^h \in \mathbf{D}_0^h(\Omega)} \|\nabla \cdot (\mathbf{u} - \mathbf{v}^h)\|_0 \leq Ch^r \|\nabla \cdot \mathbf{u}\|_r$$

for all minimization spaces $\mathbf{D}_0^h(\Omega)$ in (3.16). Likewise, (3.15) and (2.15) imply

$$\|\nabla \times \mathbf{u} - \pi_C(\nabla \times \mathbf{u})\|_0 \leq Ch^r \|\nabla \times \mathbf{u}\|_r$$

for all auxiliary spaces $\mathbf{C}_0^h(\Omega)$ in (3.16). This proves the first assertion of the corollary. Assuming that \mathbf{u} has the additional regularity stipulated in the statement of the corollary, application of (2.14) to $\nabla \times \mathbf{u}$ gives the upper bound

$$\|\nabla \times \mathbf{u} - \pi_C(\nabla \times \mathbf{u}^h)\|_0 \leq C \begin{cases} h^{r+1} \|\nabla \times \mathbf{u}\|_{r+1} & \text{if } \mathbf{C}_0^h(\Omega) = \mathbf{C}_0^r(\Omega) \text{ or } \mathbf{C}_0^{(r+1)-}(\Omega) \\ h^{r+2} \|\nabla \times \mathbf{u}\|_{r+2} & \text{if } \mathbf{C}_0^h(\Omega) = \mathbf{C}_0^{r+1}(\Omega). \end{cases}$$

This establishes the second part of the corollary. \square

REMARK 3. *The bulk of the results in Sections 3.1 and 3.2 can be extended to hexahedral elements as long as they are affine (parallelepipeds) or nearly affine. The reason for this restriction is that properties of div and curl-conforming elements deteriorate on non-affine hexahedral elements. For example, Falk et al. [20] show that the lowest-order div-conforming Raviart-Thomas space on general hexahedral elements does not contain constants, and so, convergence may be completely lost. The situation with the lowest-order curl-conforming Nédelec space of the first kind is somewhat better because this space does contain constant vector fields. As a result, convergence in L^2 for this space remains $O(h)$ on both affine and non-affine hexahedral elements; see [20]. Unfortunately, this property does not extend to the curl of the lowest-order Nédelec space which does not contain constants. Consequently, the approximation of $\nabla \times \mathbf{u}$ is suboptimal. Numerical results in Section 5.1 compare and contrast convergence of LSFEMs on affine and non-affine hexahedral elements. For further details and possible workarounds we refer to [20] and the references therein.*

4. Implementation and solution of algebraic systems.

4.1. Discrete System. The LSFEMs (3.3) and (3.4) defined in Section 3 require discrete divergence and curl operators that, in general, are represented by dense matrices. Thus, formally, the least-squares linear algebraic systems involve dense symmetric matrices. On the other hand, discrete norm-equivalence of the associated least-squares functionals, established by Theorem 3.1, implies that these matrices are also positive definite. This valuable computational property enables efficient iterative solution of least-squares linear systems and means that the matrices need not be fully assembled. This observation is key to efficient implementation and solution of least-squares linear systems.

For clarity we present the details for (3.3) and (3.4) implemented using the lowest-order finite element DeRham complex on tetrahedral³ and hexahedral elements. In this case $G_0^h(\Omega) = G_0^1(\Omega)$ is a C^0 piecewise linear (trilinear) space, $\mathbf{C}_0^h(\Omega) = \mathbf{C}_0^1(\Omega)$ is the lowest-order Nédélec edge element of the first-kind [31], $\mathbf{D}_0^h(\Omega) = \mathbf{D}_0^1(\Omega)$ is the lowest-order Raviart-Thomas [36] face element and $S_0^h(\Omega)$ is a piecewise constant space. We remind (see Remark 3) that on hexahedral elements the optimal error estimates from Section 3.2 are valid only when the elements are affine or nearly affine.

To define the linear systems some additional notation is needed. For simplicity we set all weights to one. Let $\{g_i\}$, $\{\mathbf{c}_i^h\}$, $\{\mathbf{d}_i^h\}$, and $\{s_i\}$ denote standard bases for $G_0^h(\Omega)$, $\mathbf{C}_0^h(\Omega)$, $\mathbf{D}_0^h(\Omega)$, and $S_0^h(\Omega)$, respectively, and define

$$\begin{aligned} (\mathbb{M}_C)_{ij} &= \int_{\Omega} \mathbf{c}_i \cdot \mathbf{c}_j \, d\Omega, & (\mathbb{K}_C)_{ij} &= \int_{\Omega} (\nabla \times \mathbf{c}_i) \cdot (\nabla \times \mathbf{c}_j) \, d\Omega, \\ (\mathbb{M}_D)_{ij} &= \int_{\Omega} \mathbf{d}_i \cdot \mathbf{d}_j \, d\Omega, & (\mathbb{K}_D)_{ij} &= \int_{\Omega} (\nabla \cdot \mathbf{d}_i)(\nabla \cdot \mathbf{d}_j) \, d\Omega, \\ (\mathbb{M}_G)_{ij} &= \int_{\Omega} g_i g_j \, d\Omega & (\mathbb{M}_S)_{ij} &= \int_{\Omega} s_i s_j \, d\Omega. \end{aligned} \quad (4.1)$$

Finally, let \mathbb{D}_k denote the incidence matrix⁴ between the k - and $k+1$ -dimensional facets of the mesh \mathcal{T}_h .

Consider first the curl-conforming LSFEM (3.3). In the usual manner we see that the Euler-Lagrange equation (3.10) for this LSFEM corresponds to a linear system with matrix

$$\mathbb{K}_{C^*D^*} = \mathbb{K}_C + \mathbb{K}_{D^*}, \quad (4.2)$$

where \mathbb{K}_C is curl-curl matrix defined in (4.1) and \mathbb{K}_{D^*} is a div-div matrix corresponding to the discrete divergence operator (2.17). In [7,8] it is shown that $\mathbb{K}_C = \mathbb{D}_1^T \mathbb{M}_D \mathbb{D}_1$, $\mathbb{K}_{D^*} = \mathbb{M}_C \mathbb{D}_0 \mathbb{M}_G^{-1} \mathbb{D}_0^T \mathbb{M}_C$, and

$$\mathbb{K}_{C^*D^*} = \mathbb{D}_1^T \mathbb{M}_D \mathbb{D}_1 + \mathbb{M}_C \mathbb{D}_0 \mathbb{M}_G^{-1} \mathbb{D}_0^T \mathbb{M}_C = \mathbb{M}_C \mathbb{L}_C \quad (4.3)$$

where \mathbb{L}_C is the discrete Hodge Laplacian acting on curl-conforming elements $\mathbf{C}_0^h(\Omega)$; see [6, p.575]. Multilevel methods for the solution of \mathbb{L}_C are developed in [7]. We use these methods to solve the linear systems engendered by (3.3).

The div-conforming LSFEM (3.4) leads to similar linear systems. The Euler-Lagrange equation for this LSFEM corresponds to an algebraic problem with matrix

$$\mathbb{K}_{C^*D} = \mathbb{K}_{C^*} + \mathbb{K}_D, \quad (4.4)$$

where \mathbb{K}_D is “div-div” matrix defined in (4.1) and \mathbb{K}_{C^*} is a curl-curl matrix corresponding to the discrete curl operator (2.17). Also in [7,8] it is shown that $\mathbb{K}_{C^*} = \mathbb{M}_D \mathbb{D}_1 \mathbb{M}_C^{-1} \mathbb{D}_1^T \mathbb{M}_D$, $\mathbb{K}_D = \mathbb{D}_2^T \mathbb{M}_S \mathbb{D}_2$, and

$$\mathbb{K}_{C^*D} = \mathbb{M}_D \mathbb{D}_1 \mathbb{M}_C^{-1} \mathbb{D}_1^T \mathbb{M}_D + \mathbb{D}_2^T \mathbb{M}_S \mathbb{D}_2 = \mathbb{M}_D \mathbb{L}_D, \quad (4.5)$$

where \mathbb{L}_D is discrete Hodge Laplacian acting on $\mathbf{D}_0^h(\Omega)$. Multilevel methods for \mathbb{L}_D are developed in [9]. We use these methods for the linear systems engendered by (3.4).

³These finite element spaces are also known as Whitney elements [11].

⁴For instance, \mathbb{D}_0 is the node to edge incidence matrix.

REMARK 4. *The positive definiteness of (4.2) and (4.4) follows from (3.7) and (3.8), respectively. It turns out that these matrices possess an even stronger property, namely, one can show that the size of their kernels equals the size of the kernel of the analytic Hodge Laplacian; see [7, Theorem 3.1]. This is key to formulation of efficient multilevel solvers for discrete Hodge Laplacians in [7, 9].*

Note that discrete divergence and curl operators lead to the appearance of an *inverse* mass matrix as one of the factors in \mathbb{K}_{CD^*} and \mathbb{K}_{C^*D} . Formally, this means that \mathbb{K}_{CD^*} and \mathbb{K}_{C^*D} are dense which makes their assembly and storage impossible for all but very small problems.

However, in practice, we do not have to use consistent mass matrices. In the lowest-order case, it suffices to replace \mathbb{M}_G and \mathbb{M}_C by diagonal *lumped-mass* versions $\tilde{\mathbb{M}}_G$ and $\tilde{\mathbb{M}}_C$, respectively, as long as the latter are $O(h)$ approximations of the consistent mass matrices. This does not destroy the accuracy of LSFEMs and leads to modified linear systems for which $\tilde{\mathbb{K}}_{CD^*}$ and $\tilde{\mathbb{K}}_{C^*D}$ are replaced by

$$\tilde{\mathbb{K}}_{CD^*} = \mathbb{D}_1^T \mathbb{M}_D \mathbb{D}_1 + \mathbb{M}_C \mathbb{D}_0 \tilde{\mathbb{M}}_G^{-1} \mathbb{D}_0^T \mathbb{M}_C$$

and

$$\tilde{\mathbb{K}}_{C^*D} = \mathbb{M}_D \mathbb{D}_1 \tilde{\mathbb{M}}_C^{-1} \mathbb{D}_1^T \mathbb{M}_D + \mathbb{D}_2^T \mathbb{M}_S \mathbb{D}_2,$$

respectively. The modified matrices have the usual sparse structure and their assembly and storage do not pose any problems. Moreover, the analyses in [7, 9] include inexact mass matrices so that the algebraic preconditioners from these papers can be applied to solve the modified systems.⁵

4.2. Algebraic multigrid for least-squares systems. Our algebraic multigrid (AMG) approach is derived from the earlier work in [7, 9]. Likewise, we adopt their central insight — transform a challenging problem into a well-understood one. In this case we desire to transform our conformal least-squares system on edges or faces into a coarse nodal Laplace problem, as textbook multigrid methods are very effective for nodal Laplacians. We follow a modified smoothed aggregation approach to generate our coarse problem. Smoothed aggregation is a widely available AMG method for second order elliptic systems and is described in [42, 43].

For the curl-conforming case, we note that $\tilde{\mathbb{K}}_{CD^*}$ is equal to the (1,1) block term in (5.2) of [7], once the isolated mass matrix, \mathbb{M}_C in our notation, is removed. Because this mass matrix is absent, we do not need to consider block preconditioners and hybrid smoothers which are used in the eddy current case [7, 24].

We can simply apply a coarsening algorithm similar to that which [7] propose for the (1,1) block. It is trivial to verify that near-nullspace is identical to (4.12) of [7], which means that we can use the prolongator shown in Algorithm 1 of [7] as is. This now allows us to form a coarse Laplace-like system to which a standard nodal AMG technique can be applied.

For the div-conforming case, $\tilde{\mathbb{K}}_{C^*D}$ is equal to the (1,1) block term in (3.6) of [9] once the isolated mass matrix, \mathbb{M}_D in our notation, is removed. Again, no block

⁵An alternative approach that can be used in more general settings for higher-order elements is to implement iterative solvers in an assembly-free manner. In this case, we only need the action of \mathbb{K}_{CD^*} and \mathbb{K}_{C^*D} and not the matrices themselves. Computing the action of these matrices requires the inversion of \mathbb{M}_G^{-1} and \mathbb{M}_C^{-1} that can be done using an internal conjugate gradient loop. Because \mathbb{M}_G^{-1} and \mathbb{M}_C^{-1} are well-conditioned and we do not need their inverses computed to machine precision, this requires only a few conjugate gradient iterations.

preconditioning or hybrid smoothing is required. Rather than explicitly form a near-nullspace from vectors, we follow Algorithm 1 of [9] by using the Π_h^{div} operator as in [4, 25] to interpolate a standard nodal prolongator to the faces.

In both cases, we omit prolongator smoothing on this level in order to minimize the operator complexity of the resulting preconditioner. It is well known that mesh independent convergence can be achieved when prolongator smoothing is omitted in two-level domain decomposition methods (see [29, 30, 39–41]). Thus it is reasonable to expect a similar result in this case.

4.2.1. Matrix-light smoothing. Unlike the eddy current case, which is the focus of [7], we can not omit the smoothing on either the $\tilde{\mathbb{K}}_{CD^*}$ or $\tilde{\mathbb{K}}_{C^*D}$ systems. These systems are on the finest level and thus smoothing is a necessity. We would also prefer to avoid explicitly forming the second term of $\tilde{\mathbb{K}}_{CD^*}$ (or the first term of $\tilde{\mathbb{K}}_{C^*D}$), since even with the lumped-mass versions $\tilde{\mathbb{M}}_G$ and $\tilde{\mathbb{M}}_C$, respectively, these terms still have a very large stencil. This means that the necessary matrix-matrix multiplies would be expensive in both memory use and time.

We propose the use of Chebyshev relaxation methods for the finest level smoothers in both cases [38, Algorithm 12.1]. These methods are effective at smoothing on single CPU machines and scale very well in parallel [1]. More importantly, they can be implemented in a fashion that requires two operations with the matrix — a matrix-vector product and the application of the inverse of the matrix diagonal (or some approximation thereof) for preconditioning. Our goal is to use our explicitly stored component matrices without forming the overall system. Since this is not properly a matrix-free implementation, we refer to this as a *matrix-light* approach.

The matrix-vector product is trivial to implement without explicitly forming $\tilde{\mathbb{K}}_{CD^*}$ or $\tilde{\mathbb{K}}_{C^*D}$ as the matrix-vector products are applied for each component matrix sequentially. The application of the (approximate) diagonal inverse is somewhat trickier. In the $\tilde{\mathbb{K}}_{CD^*}$ case, the diagonal of $\mathbb{D}_1^T \mathbb{M}_D \mathbb{D}_1$ is readily available, since this matrix is explicitly formed, while the diagonal of $\mathbb{M}_C \mathbb{D}_0 \tilde{\mathbb{M}}_G^{-1} \mathbb{D}_0^T \mathbb{M}_C$ is not. Likewise in the $\tilde{\mathbb{K}}_{C^*D}$ case, the diagonal of $\mathbb{D}_2^T \mathbb{M}_S \mathbb{D}_2$ is readily available, while the diagonal of $\mathbb{M}_D \mathbb{D}_1 \tilde{\mathbb{M}}_C^{-1} \mathbb{D}_1^T \mathbb{M}_D$ is not.

Approximating the diagonal of a matrix is a problem that has been studied in several contexts [5, 18] and such general techniques can be easily applied for our problems. These methods are usually based on the application of a number of matrix-vector products to sample the diagonal during the algorithm setup phase, which adds expense. We also propose an alternative approach for this particular system.

If we assume that material constants do not differ much in scale, the first and second terms in either the $\tilde{\mathbb{K}}_{CD^*}$ or $\tilde{\mathbb{K}}_{C^*D}$ matrix components should be of the same scale. One term involves two derivatives and one mass matrix. The other involves two derivatives, two mass matrices and the inverse of a third mass matrix. This means that in the finite element case they should both be $O(h^{-1})$. Approximating the diagonal of the matrix we do not explicitly have with a constant multiple of the one we do have works well for orthogonal meshes, even when they are stretched. For non-orthogonal meshes, a slightly more complicated method is required.

In the $\tilde{\mathbb{K}}_{CD^*}$ case, we form the actual diagonal of the matrix $\mathbb{M}_C \mathbb{D}_0 \tilde{\mathbb{M}}_G^{-1} \mathbb{D}_0^T \mathbb{M}_C$ where \mathbb{M}_C is replaced by its diagonal. Rather than requiring four matrix-matrix multiplies as the above equation would suggest, this can be done with only one matrix-matrix multiply. The following MATLAB code illustrates this approach for both curl

and div-conforming elements:

$$D_C = \text{diag} \left(\text{diag} (\mathbb{D}_1^T \mathbb{M}_D \mathbb{D}_1) + (\text{abs}(\mathbb{D}_0) * \text{diag}(\mathbb{M}_G)) . * (\text{diag}(\mathbb{M}_C).^2) \right); \quad (4.6)$$

$$D_D = \text{diag} \left(\text{diag} (\mathbb{D}_2^T \mathbb{M}_S \mathbb{D}_2) + (\text{abs}(\mathbb{D}_1) * \text{diag}(\mathbb{M}_C)) . * (\text{diag}(\mathbb{M}_D).^2) \right); \quad (4.7)$$

We demonstrate the appropriateness of this approach, even in the case of unstructured meshes, in Section 5.2.

5. Numerical results. We consider three model problems for testing the LS-FEM formulations and proposed solvers. Our first test problem involves solving (1.1) and (1.2) on the orthogonal box $[-1, 1]^3$ using uniform hexahedral elements, i.e., elements whose faces are squares. For simplicity we take $\Theta_0 = 1$ and Θ_1 and Θ_2 equal to the identity. We use this test problem for both order of convergence studies as well as solver scalability. In both cases, the mesh is uniformly refined from 10^3 to 80^3 and all elements are affine. We refer to this problem as the orthogonal box problem.

The second model problem has the same geometry as the first, except that we set material parameter Θ_1 to a multiple of the identity with coefficient c . Inside of the box $[-0.5, 0.5]^3$, c is varied between $1e-2$ to $1e2$, while the remainder of the domain ($[-1, 1]^3 \setminus [-0.5, 0.5]^3$) has $c = 1$. As before, we take $\Theta_0 = 1$ and Θ_2 equal to the identity. Here we uniformly refined the mesh from 10^3 to 80^3 . We refer to this as the “box-in-a-box” problem. Again, all elements in this setting are affine.

Our final model problem involves a distorted mesh with *non-affine* hexahedral elements. Unstructured and semi-structured meshes often cause challenges for linear solvers because the meshes can contain elements with poor aspect ratios or small angles. Therefore, the main purpose of this problem is to test the performance of the solvers described in Section 4. Additionally, we use this setting to illustrate the convergence issues with curl and div-conforming elements that were mentioned in Remark 3. We consider the following model distorted mesh shown in Figure 5.1. Note

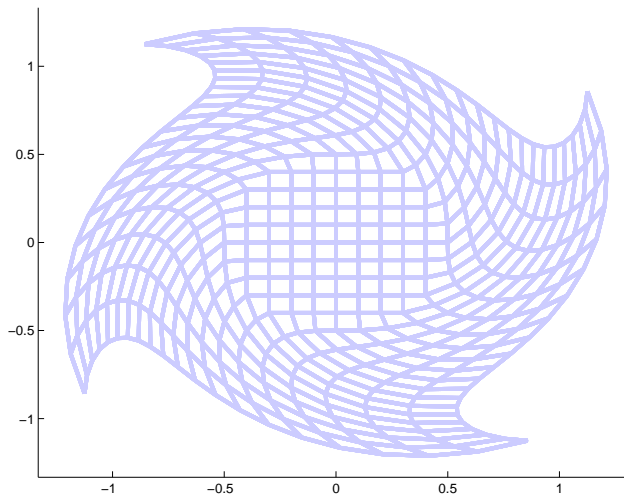


FIG. 5.1. 2D (x - y) projection of the 3D model distorted mesh problem at the coarsest grid resolution.

that the center of the mesh is basically orthogonal, while the elements near the corners have been seriously distorted. This mesh is created by distorting an orthogonal box

	Mesh Size			
	10 ³	20 ³	40 ³	80 ³
$\ \mathbf{u} - \mathbf{u}^h\ _0$	0.31318	0.13991	0.067749	0.033597
Order of Convergence	1.1625	1.0462	1.0119	
$\ \nabla \cdot \mathbf{u} - \nabla \cdot \mathbf{u}^h\ _0$	2.3036	1.1575	0.57905	0.28945
Order of Convergence	0.9929	0.9993	1.0003	

TABLE 5.1

Error and order of convergence for manufactured solution on box mesh using \mathbf{C}^{1-} .

where the coordinates are remapped as follows,

$$\begin{aligned}
 r &\leftarrow \sqrt{x_0^2 + y_0^2}, \\
 \theta &\leftarrow \text{atan2}(x_0, y_0), \\
 \begin{bmatrix} x \\ y \end{bmatrix} &\leftarrow \begin{cases} \begin{bmatrix} x_0 \\ y_0 \end{bmatrix} & \text{if } r \leq 0.5 \\ \begin{bmatrix} r \cos\left(\theta + \frac{(r-.5)\pi}{2}\right) \\ r \sin\left(\theta + \frac{(r-.5)\pi}{2}\right) \end{bmatrix} & \text{if } r > 0.5 \end{cases}.
 \end{aligned}$$

The z coordinate remains unchanged. We keep the mesh in the z -direction a factor of 2.5 coarser than the mesh in the x and y directions in order to create additional mesh anisotropy in the problem. The meshing and distortion is done automatically using Pamgen, a part of the Trilinos library collection [22, 23]. We take $\Theta_0 = 1$ and Θ_1 and Θ_2 equal to the identity and refer to this as the distorted mesh problem.

5.1. Order of convergence study. To test the order of convergence we solve the orthogonal box and distorted mesh problems using manufactured solutions. In the curl-compatible case, we assume an exact solution \mathbf{u} given by

$$\mathbf{u} = \begin{pmatrix} \exp(x + y + z)(y^2 - 1)(z^2 - 1) \\ \exp(x + y + z)(x^2 - 1)(z^2 - 1) \\ \exp(x + y + z)(x^2 - 1)(y^2 - 1) \end{pmatrix}. \quad (5.1)$$

This solution satisfies the homogeneous boundary conditions in (1.1). The right-hand side functions, \mathbf{g} and f from (1.1) are obtained by substituting the exact solution in (5.1) into the differential equations. These functions are used to generate data for the right-hand side of the discrete linear system. In the curl-conforming case the right hand side vector, \mathbf{b} , is formed from the terms $(\mathbf{g}, \nabla \times \mathbf{u}^h) + (f, \nabla^* \cdot \mathbf{u}^h)$. We use integration by parts on the second term to remove the weak divergence of \mathbf{u}^h . This introduces a boundary term, which depends on the boundary normal, \mathbf{n} . As a function of the curl-conforming basis, $\{\mathbf{c}_i\}$, components of the right-hand side vector are then calculated as

$$\mathbf{b}_i = \int_{\Omega} \mathbf{g} \cdot (\nabla \times \mathbf{c}_i) d\Omega - \int_{\Omega} \nabla f \cdot \mathbf{c}_i d\Omega + \int_{\Gamma} f \mathbf{c}_i \cdot \mathbf{n} d\Gamma. \quad (5.2)$$

For these test cases the lowest order Nédelec edge element, \mathbf{C}^{1-} is used. In Table 5.1 results from the convergence study for the curl-compatible case on the *affine* box grid are shown and first order-convergence, as expected from Corollary 3.3, is seen.

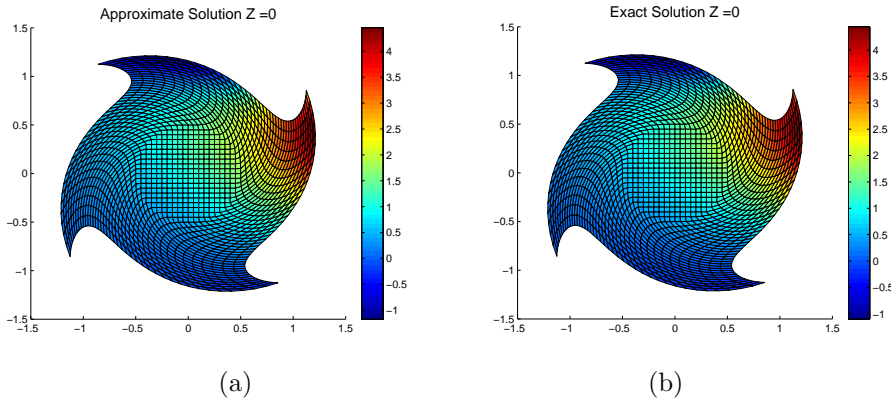


FIG. 5.2. Slice through the center of the $40 \times 40 \times 16$ distorted mesh in the $(x-y)$ plane displaying (a) approximate and (b) exact x -component of solution for the curl-conforming LSFEM.

	Mesh Size		
	$10 \times 10 \times 4$	$20 \times 20 \times 8$	$40 \times 40 \times 16$
$\ \mathbf{u} - \mathbf{u}^h\ _0$	0.89131	0.420695	0.212596
Order of Convergence		1.0832	0.98466
$\ \nabla \times \mathbf{u} - \nabla \times \mathbf{u}^h\ _0$	4.89925	2.73187	1.55896
Order of Convergence		0.84267	0.80930

TABLE 5.2

Error and order of convergence for manufactured solution on distorted mesh using \mathbf{C}^1 .

A convergence test was also performed for the *non-affine* distorted mesh using the exact solution in (5.1). On the distorted mesh, this function does not satisfy homogeneous boundary conditions and, therefore, boundary conditions of the form $\mathbf{u} \times \mathbf{n} = \tilde{\mathbf{u}}$, where $\tilde{\mathbf{u}}$ is calculated from the exact solution, were applied. Figure 5.2 shows a slice through the $40 \times 40 \times 16$ distorted mesh with the x -component of the approximate and exact solutions. Convergence results are shown in Table 5.2. The data in this table is consistent with the comments made in Remark 3. Specifically, we see that the optimal order of convergence is preserved in the L^2 norm but is reduced in the $H(\text{curl})$ semi-norm, as it should for the lowest-order Nédélec space on non-affine hexahedral elements.

Similar calculations were performed for the div-conforming case, where the exact solution \mathbf{u} is given by

$$\mathbf{u} = \begin{pmatrix} \exp(y+z)(x^2-1) \\ \exp(x+z)(y^2-1) \\ \exp(x+y)(z^2-1) \end{pmatrix}. \quad (5.3)$$

This function was chosen to satisfy the homogeneous boundary conditions given in (1.2). The right-hand side terms are derived from this function in the usual manner by substituting the exact solution into the differential equations. In the div-conforming case the right-hand side vector is generated from $(\mathbf{g}, \nabla^* \times \mathbf{u}^h) + (f, \nabla \cdot \mathbf{u}^h)$. Integration by parts is used here to remove the weak curl from the first term, which introduces a boundary term. As a function of the components of the div-conforming basis, $\{\mathbf{d}_i\}$,

	Mesh Size			
	10^3	20^3	40^3	80^3
$\ \mathbf{u} - \mathbf{u}^h\ _0$	0.529424	0.265879	0.132593	0.066244
Order of Convergence	0.99365	1.0038	1.0011	
$\ \nabla \cdot \mathbf{u} - \nabla \cdot \mathbf{u}^h\ _0$	1.76578	0.858779	0.428503	0.213946
Order of Convergence	1.0399	1.0030	1.0021	

TABLE 5.3

Error and order of convergence for manufactured solution on box mesh using \mathbf{D}^{1-} .

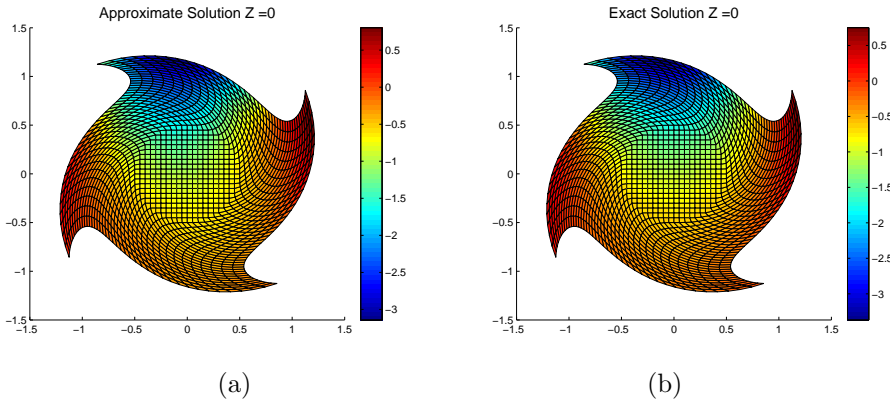


FIG. 5.3. Slice through the center of the $40 \times 40 \times 16$ distorted mesh in the $(x-y)$ plane displaying (a) approximate and (b) exact x -component of solution for the div-conforming case.

the components of the right-hand side vector are calculated as

$$\mathbf{b}_i = - \int_{\Omega} \nabla \times \mathbf{g} \cdot \mathbf{d}_i d\Omega + \int_{\Gamma} (\mathbf{g} \times \mathbf{d}_i) \cdot \mathbf{n} d\Gamma + \int_{\Omega} f \nabla \cdot \mathbf{d}_i d\Omega. \quad (5.4)$$

The lowest order Raviart-Thomas element, \mathbf{D}^{1-} was used for the div-conforming calculations and first-order convergence on the *affine* box mesh is seen as predicted from Corollary 3.5. The convergence results are shown in Table 5.3.

Another convergence test was performed for the *non-affine* distorted mesh using the exact solution in (5.3) and \mathbf{D}^{1-} elements. As in the curl-conforming case, this function does not satisfy homogeneous boundary conditions on the distorted mesh and therefore the exact solution was used to calculate boundary values.

Figure 5.3 shows a slice through the $40 \times 40 \times 16$ distorted mesh with the x -component of the approximate and exact solutions. In the “eyeball” norm the two solutions appear well-matched and very similar. However, the convergence results, shown in Table 5.4, reveal that convergence in L^2 is essentially lost, while the order of the $H(\text{div})$ -seminorm error is significantly reduced. This behavior is in line with the comments made in Remark 3 about div-conforming elements on non-affine hexahedral grids. To avoid loss of convergence either tetrahedral elements or a higher-order basis on hexahedral elements could be used.

5.2. Solver scalability. We consider five different variants of the solver described in Section 4.2. All of these involve different methods of estimating the diagonal of the $\tilde{\mathbb{K}}_{CD^*}$ or $\tilde{\mathbb{K}}_{C^*D}$ matrix for Chebyshev smoothing. The first method, denoted “Baseline” involves explicitly forming the “addon” matrix $(\mathbb{M}_C \mathbb{D}_0 \tilde{\mathbb{M}}_G^{-1} \mathbb{D}_0^T \mathbb{M}_C$ in the

	Mesh Size		
	$10 \times 10 \times 4$	$20 \times 20 \times 8$	$40 \times 40 \times 16$
$\ \mathbf{u} - \mathbf{u}^h\ _0$	1.91489	1.48594	1.42005
Order of Convergence	0.36589	0.06543	
$\ \nabla \cdot \mathbf{u} - \nabla \cdot \mathbf{u}^h\ _0$	4.60218	3.05206	2.07471
Order of Convergence	0.59253	0.55687	

TABLE 5.4

Error and order of convergence for manufactured solution on distorted mesh using \mathbf{D}^{1-} .

$\tilde{\mathbb{K}}_{CD^*}$ case, or $\mathbb{M}_D \mathbb{D}_1 \tilde{\mathbb{M}}_C^{-1} \mathbb{D}_1^T \mathbb{M}_D$ in the $\tilde{\mathbb{K}}_{C^*D}$ case) in order to extract the diagonal. This method is not tenable in practice, due to the expense, but establishes a minimum baseline for the number of iterations. Barring the occasional stroke of luck, no other method should perform better than this one.

The second method involves the proposed diagonal approximations detailed in (4.6) and (4.7). They are denoted “Estimate (4.6)” and “Estimate (4.7),” respectively. The performance of these methods ought to be close to that of the Baseline method, but at significantly reduced expense.

The third method is denoted “Stiffness Only.” In the context of the eddy current approximation to Maxwell’s equations, it has been theorized that adding a stabilization term (e.g. $\mathbb{M}_C \mathbb{D}_0 \tilde{\mathbb{M}}_C^{-1} \mathbb{D}_0^T \mathbb{M}_C$ in the curl-conforming case) is not necessary in the positive definite case (4.6) [7]. We use this method to test to see if that hypothesis applies to least-squares systems as well.

The fourth and fifth methods are implementations of “Diagonal Estimator” algorithm described as the baseline for comparison in Section 2.1 of [5]. These variants are referred to as “Random(10)” and “Random(15),” and respectively use 10 and 15 randomly generated vectors to approximate the diagonal of the matrix.

For all of the below problems, a single V-cycle of the aforementioned solvers is accelerated with CG with a tolerance of $1e - 10$. Two pre and post smoothing steps of Chebyshev are run at each level of the V-cycle. We run at most 200 iterations of each of the above solvers and any method that has not met the specified tolerance is reported as having not converged. All of these experiments are run in MATLAB using ML’s mlmex interface [21] as a sub-solver for the coarse vector Laplace problems.

5.2.1. Curl-conforming orthogonal box. We consider the five solvers described in Section 5.2. These results are shown in Table 5.5. We first note that the “Stiffness Only” method has severe convergence issues. This implies that the use of the “addon” term (i.e. $\mathbb{M}_C \mathbb{D}_0 \tilde{\mathbb{M}}_C^{-1} \mathbb{D}_0^T \mathbb{M}_C$ in the curl-conforming case) is necessary for least-squares systems. This contrasts with previous results on the eddy current Maxwell’s equations, where such a term was not necessary in the positive definite case [7].

Secondly, we note that the baseline method has good convergence properties with respect to mesh refinement. This relatively flat scaling (after the 10^3 mesh) suggests that the baseline method is delivering some modicum of mesh independence.

Finally, we note that the diagonal estimate using (4.6) yields convergence results practically identical to the baseline method of explicitly forming the system matrix. This indicates that (4.6) is a practical, reliable estimate of the diagonal for the cost of only one matrix-vector product. This contrasts with the results from the random diagonal estimation, which needs 15 matrix-vector multiplies to perform near the level of the random diagonal estimation.

Diagonal	Mesh Size			
	10	20	40	80
Baseline	18	24	22	25
Estimate (4.6)	18	24	22	25
Stiffness Only	140	*	*	*
Random(10)	49	108	90	*
Random(15)	20	25	34	142

TABLE 5.5

Multigrid solver iterations for curl-conforming LSFEM on an orthogonal box of size 10^3 to 80^3 (* indicates that method did not converge in 200 iterations).

Diagonal	1e-2			1e-1			1e0		
	10	20	40	10	20	40	10	20	40
Baseline	46	70	83	20	29	33	18	24	22
Estimate (4.6)	48	71	84	20	29	33	18	24	22
Random(10)	135	*	*	56	126	115	49	107	88
Random(15)	54	78	111	23	31	44	20	25	34

Diagonal	1e1			1e2		
	10	20	40	10	20	40
Baseline	21	30	31	43	68	78
Estimate (4.6)	21	30	32	43	69	78
Random(10)	55	131	109	125	*	*
Random(15)	22	32	41	49	85	98

TABLE 5.6

Multigrid solver iterations for curl-conforming LSFEM on an orthogonal box of size 10^3 to 80^3 (* indicates that method did not converge in 200 iterations).

5.2.2. Curl-conforming variable materials. Given the level of performance of the “Stiffness Only” method in Section 5.2.1 we remove it from consideration for the variable materials problem. Table 5.6 shows the convergence results with variable Θ_1 . We note again that the method of (4.6) yields convergence results very similar to the baseline method and substantially better than either of the random methods.

5.2.3. Curl-conforming distorted mesh. Table 5.7 details solver convergence for uniform mesh refinement on the distorted mesh shown in Figure 5.1. We note that while convergence does deteriorate with respect to mesh refinement (due to the poor quality of the mesh), using the diagonal estimate of (4.6) yields convergence behavior almost identical to that of explicitly forming the diagonal. We do not report results for either the random or stiffness only cases. In these cases, the method fails to converge within our budget of 200 iterations.

5.2.4. Div-conforming orthogonal box. Much as in Section 5.2.1, we consider five solvers described in Section 5.2. These results are shown in Table 5.8. First, we note that the “Stiffness Only” method does not converge to the specified tolerance for any problem size. This implies that the use of the “addon” term (i.e. $\mathbb{M}_D \mathbb{D}_1 \tilde{\mathbb{M}}_C^{-1} \mathbb{D}_1^T \mathbb{M}_D$) is necessary for rapid solution on div-conforming LSFEMs.

Second, we note that the baseline method has very good performance with respect to mesh refinement. This suggests that convergence may be bounded in a mesh-

Diagonal	Mesh Size		
	$20 \times 20 \times 8$	$40 \times 40 \times 16$	$80 \times 80 \times 32$
Explicit	53	93	116
Estimate (4.6)	53	96	120

TABLE 5.7

Multigrid solver iterations for curl-conforming LSFEM on a distorted mesh size $20 \times 20 \times 8$ to $80 \times 80 \times 32$.

Diagonal	Mesh Size			
	10	20	40	80
Baseline	17	21	20	22
Estimate (4.7)	18	21	20	22
Stiffness Only	*	*	*	*
Random(10)	20	99	*	*
Random(15)	18	32	172	70

TABLE 5.8

Multigrid solver iterations for div-conforming LSFEM on an orthogonal box of size 10^3 to 80^3 (* indicates that the method did not converge in 200 iterations).

independent fashion. Likewise, we note that the method using the diagonal estimate of (4.7) is nearly identical to the baseline approach. This indicates that (4.7) is a practical, reliable estimate of the diagonal for the cost of only one matrix-vector product. The performance of the random diagonal estimation methods is very poor even in the 15 vector case.

5.2.5. Div-conforming variable materials. Much as in the curl-conforming case, the performance of the “Stiffness Only” method in Section 5.2.4 is very poor, so we remove it from consideration for the variable materials problem. Table 5.9 shows the convergence results with variable Θ_1 . We note that except in the cases of a small coefficient for Θ_1 the method of (4.7) yields convergence results very similar to baseline method. The random methods perform both quite poorly, especially for coefficients that are less than one.

5.2.6. Div-conforming distorted mesh. Table 5.10 details solver convergence for uniform mesh refinement on the distorted mesh shown in Figure 5.1. Much as in the curl-conforming case, the convergence deteriorates with respect to mesh refinement (due to the poor quality of the mesh). However using the diagonal estimate of (4.6) yields convergence behavior almost identical to that of explicitly forming the diagonal. As above, we have do not report results for either the random or stiffness only cases as those methods fail to converge within our budget of 200 iterations.

6. Conclusions. A strategy for solving div-curl systems using least-squares methods has been presented. The stability of the “partially” conforming discretization has been proved and error estimates were derived. Numerical results show optimal convergence of both the curl-conforming and div-conforming discretizations on the regular box mesh. However, on the distorted mesh the optimal convergence is not obtained for the lowest-order basis functions. Although the linear systems generated from these discretizations involve non-sparse matrices, these matrices are symmetric and positive definite and can be solved efficiently with our proposed AMG method.

Diagonal	$1e-2$			$1e-1$			$1e0$		
	10	20	40	10	20	40	10	20	40
Baseline	75	114	142	25	38	47	16	19	19
Estimate (4.6)	92	151	191	25	39	47	16	19	19
Random(10)	*	*	*	46	*	*	18	133	*
Random(15)	*	*	*	38	69	*	16	21	25

Diagonal	$1e1$			$1e2$		
	10	20	40	10	20	40
Baseline	16	19	20	38	46	48
Estimate (4.6)	16	19	20	36	46	48
Random(10)	18	125	*	43	*	*
Random(15)	16	21	25	38	46	52

TABLE 5.9

Multigrid solver iterations for div-conforming LSFEM on an orthogonal box of size 10^3 to 40^3 , with a coefficient, c , of Θ_1 varied from $1e-2$ to $1e2$ (* indicates that method did not converge in 200 iterations).

Diagonal	Mesh Size		
	$20 \times 20 \times 8$	$40 \times 40 \times 16$	$80 \times 80 \times 32$
Baseline	50	79	124
Estimate (4.7)	50	82	130

TABLE 5.10

Multigrid solver iterations for div-conforming LSFEM on a distorted mesh size $20 \times 20 \times 8$ to $80 \times 80 \times 32$.

Acknowledgments. We would like to thank David Hensinger for assistance with meshing in Pamgen and providing us with our distorted mesh test problem.

REFERENCES

- [1] M. Adams, M. Brezina, J. Hu, and R. Tuminaro. Parallel multigrid smoothing: polynomial versus Gauss-Seidel. *J. Comp. Phys.*, 188:593–610, 2003.
- [2] P. Alotto and I. Perugia. A field-based finite element method for magnetostatics derived from an error minimization approach. *Int. J. Numer. Meth. Eng.*, 49(4):573–598, 2000.
- [3] D. N. Arnold, R. S. Falk, and R. Winther. Finite element exterior calculus, homological techniques, and applications. Technical Report 2094, Institute for Mathematics and Its Applications, 2006.
- [4] R. Beck. Algebraic multigrid by component splitting for edge elements on simplicial triangulations. Technical Report SC 99-40, Zuse Institute Berlin, December 1999.
- [5] C. Bekas, E. Kokiopoulou, and Y. Saad. An estimator for the diagonal of a matrix. *Appl. Numer. Math.*, 57:1214–1229, 2007.
- [6] P. Bochev and M. Gunzburger. *Least-Squares finite element methods*, volume 166 of *Applied Mathematical Sciences*. Springer Verlag, 2009.
- [7] P. Bochev, J. Hu, C. Siefert, and R. Tuminaro. An algebraic multigrid approach based on a compatible gauge reformulation of Maxwells equations. *SIAM J. Sci. Comp.*, 31(1):557–583, 2008. Published online 10/31/2008.
- [8] P. Bochev and M. Hyman. Principles of compatible discretizations. In D. N. Arnold, P. Bochev, R. Lehoucq, R. Nicolaides, and M. Shashkov, editors, *Compatible Discretizations, Proceedings of IMA Hot Topics Workshop on Compatible Discretizations*, volume IMA 142, pages 89–120. Springer Verlag, 2006.
- [9] P. Bochev, C. Siefert, R. Tuminaro, J. Xu, and Y. Zhu. Compatible gauge approaches for $H(\text{div})$ equations. In M. Parks and S. Collis, editors, *Computer Science Research Institute*

- Summer Proceedings*, pages 3–14, 2007.
- [10] A. Bossavit. Mixed finite elements and the complex of Whitney forms. In J.R. Whiteman, editor, *The Mathematics of Finite Elements and Applications*, volume VI, pages 37–44, London, 1988. Academic Press.
 - [11] A. Bossavit. Whitney forms: A class of finite elements for three-dimensional computations in electromagnetism. *IEE Proc.*, 135(8):493–500, 1988.
 - [12] A. Bossavit. *Computational Electromagnetism*. Academic Press, San Diego, 1998.
 - [13] S. Brenner and R. Scott. *The Mathematical Theory of Finite Element Methods*. Number 15 in Texts in Applied Mathematics. Springer Verlag, New York, 2002.
 - [14] F. Brezzi and M. Fortin. *Mixed and Hybrid Finite Element Methods*. Springer, Berlin, 1991.
 - [15] F. Brezzi, D. Marini, I. Perugia, D. Di Barba, and A. Savini. A novel field-based mixed formulation of magnetostatics. *IEEE Trans. Mag.*, 32:635–638, 1996.
 - [16] S. H. Christiansen and R. Winther. Smoothed projections in finite element exterior calculus. *Math. Comp.*, 77:813–829, 2007.
 - [17] M. Costabel. A coercive bilinear form for the Maxwell’s equations. *J. Math. Anal. Appl.*, 157:527–541, 1991.
 - [18] A.R. Curtis, M.J.D. Powell, and J.K. Reid. On the estimation of sparse Jacobian matrices. *J. Inst. Math. Appl.*, 13:117–119, 1974.
 - [19] A. Ern and J.-L. Guermond. *Theory and Practice of Finite Elements*. Number 159 in Applied Mathematical Sciences. Springer Verlag, New York, 2004.
 - [20] R. S. Falk, P. Gatto, and P. Monk. Hexahedral $H(\text{div})$ and $H(\text{curl})$ finite elements. *ESAIM: Mathematical Modeling and Numerical Analysis*, Submitted, 2009.
 - [21] M.W. Gee, C.M. Siefert, J.J. Hu, R.S. Tuminaro, and M.G. Sala. ML 5.0 smoothed aggregation user’s guide. Technical Report SAND2006-2649, Sandia National Laboratories, 2006.
 - [22] D. M. Hensinger, R. R. Drake, J. G. Foucar, and T. A. Gardiner. Pamgen, a library for parallel generation of simple finite element meshes. Technical Report SAND2008-1933, Sandia National Laboratories, April 2008.
 - [23] M. A. Heroux, R. A. Bartlett, V. E. Howle, R. J. Hoekstra, J. J. Hu, T. G. Kolda, R. B. Lehoucq, K. R. Long, R. P. Pawlowski, E. T. Phipps, A. G. Salinger, H. K. Thornquist, R. S. Tuminaro, J. M. Willenbring, A. Williams, and K. S. Stanley. An overview of the Trilinos project. *ACM Trans. Math. Softw.*, 31(3):397–423, 2005.
 - [24] R. Hiptmair. Multigrid method for Maxwell’s equations. *SIAM J. Numer. Anal.*, 36:204–225, 1998.
 - [25] R. Hiptmair and J. Xu. Nodal auxiliary space preconditioning in $H(\text{curl})$ and $H(\text{div})$ spaces. *SIAM J. Numer. Anal.*, 45(6):2483–2509, 2007.
 - [26] J. Hyman and M. Shashkov. Adjoint operators for the natural discretizations of the divergence, gradient and curl on logically rectangular grids. *Appl. Num. Math.*, 25:413–442, 1997.
 - [27] J. Hyman and M. Shashkov. Natural discretizations for the divergence, gradient and curl on logically rectangular grids. *Comput. Math. Appl.*, 33:88–104, 1997.
 - [28] J. Hyman and M. Shashkov. Mimetic discretizations for Maxwell’s equations. *J. Comp. Phys.*, 151:881–909, 1999.
 - [29] E. W. Jenkins, C. E. Kees, C. T. Kelley, and C. T. Miller. An aggregation-based domain decomposition preconditioner for groundwater flow. *SIAM J. Sci. Comput.*, 23(2):430–441, 2002.
 - [30] C. Lasser and A. Toselli. Convergence of some two-level overlapping domain decomposition preconditioners with smoothed aggregation coarse spaces. In L. Pavarino and A. Toselli, editors, *Recent Developments in Domain Decomposition Methods*, volume 23 of LNCSE. Springer Verlag, 2002.
 - [31] J. C. Nédélec. Mixed finite elements in \mathbf{R}^3 . *Numerische Mathematik*, 35:315–341, 1980.
 - [32] J. C. Nédélec. A new family of finite element methods in \mathbf{R}^3 . *Numerische Mathematik*, 50:57–81, 1986.
 - [33] R. Nicolaides. Direct discretization of planar div-curl problems. *SIAM J. Numer. Anal.*, 29:32–56, 1992.
 - [34] R. Nicolaides and K. Trapp. Covolume discretizations of differential forms. In D. N. Arnold, P. Bochev, R. Lehoucq, R. Nicolaides, and M. Shashkov, editors, *Compatible Discretizations, Proceedings of IMA Hot Topics workshop on Compatible Discretizations*, volume IMA 142, pages 161–172. Springer Verlag, 2006.
 - [35] R. Nicolaides and X. Wu. Covolume solutions of three-dimensional div-curl equations. *SIAM J. Numer. Anal.*, 34:2195–2203, 1997.
 - [36] P. A. Raviart and J. M. Thomas. A mixed finite element method for second order elliptic problems. In Galligani and E. Magenes, editors, *Mathematical Aspects of the Finite Element Method, I*, number 606 in Lecture Notes in Math. Springer-Verlag, New York, 1977.

- [37] J. Rikabi, C. F. Bryant, and E. M. Freeman. An error-based approach to complementary formulations of static field solutions. *Int. J. Numer. Meth. Eng.*, 26(9):1963–1987, 1988.
- [38] Y. Saad. *Iterative Methods for Sparse Linear Systems*. SIAM, 2nd edition, 2003.
- [39] M. Sala. *Domain Decomposition Preconditioners: Theoretical Properties, Application to the Compressible Euler Equations, Parallel Aspects*. PhD thesis, Ecole Polytechnique Fédérale de Lausanne, Switzerland, 2003.
- [40] M. Sala. Analysis of two-level domain decomposition preconditioners based on aggregation. *Mathematical Modelling and Numerical Analysis*, 38(5):765–780, 2004.
- [41] M. Sala, J. Shadid, and R. Tuminaro. An improved convergence bound for aggregation-based domain decomposition preconditioners. *SIAM J. Matrix Anal.*, 27:744–756, 2005.
- [42] P. Vaněk, M. Brezina, and J. Mandel. Convergence of algebraic multigrid based on smoothed aggregation. *Numer. Math.*, 88:559–579, 2001.
- [43] P. Vaněk, J. Mandel, and M. Brezina. Algebraic multigrid based on smoothed aggregation for second and fourth order problems. *Computing*, 56:179–196, 1996.